# 31 May 2013 El Reno Tornadoes: Forecaster's Warning Decision Process and Assessment of Storm Evolution Seen in WSR-88D and NWRT PAR Data

Pamela Heinselman[1,2], Charles Kuster[2,3], and Marcus Austin[4]

[1]*NOAA National Severe Storms Laboratory, Norman, Oklahoma,USA*
[2]*Univerisity of Oklahoma School of Meteorology, Norman, Oklahoma, USA*
[3]*Cooperative Institute for Mesoscale Meteorology, Norman, Oklahoma, USA*
[4]*NOAA National Weather Service, Norman, Oklahoma, USA*

## 1 Introduction

To better understand an unpredictable atmosphere, meteorologists create scientific conceptual models to aid in identifying favorable severe-weather environments and assist in overall threat recognition, especially in terms of supercells and tornadogenesis (e.g., Johns 1993; Doswell et al. 1996; Andra et al 2002). Scientifically based conceptual models of the environment (e.g., Johns and Doswell 1992), supercells (e.g., Doswell and Burgess 1993), and tornadogenesis (e.g., Wicker and Wilhelmson 1995) allow a forecaster to develop expectations about a given severe weather event. As storms develop, forecasters use conceptual models to anticipate future storm characteristics and develop predictions for potential hazards posed by the storms (Andra et al. 2002). These predictions act as building blocks for accurate decisions about a warning's location, timing, and type (Hahn et al. 2003). In addition, conceptual models can affect how a forecaster interprets radar data. Heinselman et al. (2012) note that forecasters lowered their thresholds for issuing tornado warnings in a tropical environment, while Lindley and Morgan (2004) discuss a reluctance by forecasters to issue tornado warnings due to their environmental conceptual models despite the presence of radar signatures supportive of tornado warnings. Matching current storm attributes to existing conceptual models therefore appears to be a key to successful anticipation of hazardous events and by extension, accurate warnings (Andra et al. 2002).

Given the importance of conceptual models in an operational setting, research efforts have focused on developing and improving conceptual models of supercells and tornadogenesis. Observations of supercells led to conceptual depictions of these storms in terms of precipitation distribution, updraft location, and basic airflow patterns (Doswell and Burgess 1993). Observations have also led to a basic classification of supercells based on their visual appearance and precipitation distribution, spanning from low-precipitation (LP) supercells (Bluestein and Parks 1983) to high-precipitation (HP) supercells (Moller et al. 1990). The knowledge provided by these conceptual models could assist forecasters in identifying potential hazards. For example, LP supercells produce fewer tornadoes on average, while HP supercells may not display noticeable hook echoes, but can contain a circulation embedded within high reflectivity (Doswell and Burgess 1993).

Conceptual models have been further advanced by numerical simulation studies that provide insight into the evolution of three-dimensional airflow within supercells prior to and during tornadogenesis (e.g., Klemp and Rotunno 1983; Wicker and Wilhelmson 1995; Adlerman et al. 1999). In particular, Wicker and Wilhelmson (1995) demonstrated the interconnections between rotation intensity, updraft strength, and low-level convergence. In their study, increased mesocyclone rotation led to a stronger upward-directed pressure gradient force, which dynamically forced a stronger updraft (Wicker and Wilhelmson 1995). This uptick in updraft strength acted to enhance existing low-level convergence along the rear-flank downdraft (RFD). In turn, stronger low-level convergence aided in increasing updraft intensity, completing the positive feedback loop. The enhanced updraft and low-level convergence aided in vorticity tilting and stretching, promoting tornadogenesis. Noting these interconnections in the conceptual model, a forecaster who observes increasing mesocyclone rotation, strong updraft pulses, and increasing low-level convergence may have greater confidence in tornado warning issuance.

A particularly important aspect in the development of conceptual models has been the advancement of radar technology that has led to changes in the models and severe-weather warning operations (e.g., Wilson et al. 1980; Vasiloff 2001; Heinselman et al. 2008). Early radar observations using new Doppler technology focused on supercell airflow related to tornadogenesis and the operational use of this data. Brandes (1978) showed the presence of strong low-level inflow during mesocyclone intensification. The tornado vortex signature (TVS) served as another indication of a storm's increased tornado potential (Brown et al. 1978). While the detection of a TVS does not guarantee surface tornadogenesis, its existence can increase confidence in the warning process, especially when the storm is closer to the radar. Early research also identified other processes within the supercell such a descending TVS (Lemon et al. 1978) and the RFD (Brandes 1984) that can signal an increase in tornado potential to a forecaster.

Concurrently, research was being conducted with National Weather Service (NWS) forecasters to determine the operational uses and benefits of Doppler radar technology. The Joint Doppler Operational Project (e.g., Burgess et al. 1979) examined the operational benefits of Doppler radar in observing storm characteristics such as storm-top divergence and mesocyclones. The study found that tornado warnings issued using this new technology had longer lead times and lower false alarm rates than those issued using only the Weather Surveillance Radar – 1957 network. A study conducted by Dunn (1990) revealed similar results by exploring the impacts of Doppler radar on two operational case studies. The new technology revealed clear circulations located in an echo free region beneath a high reflectivity overhang that confirmed the existence of a rotating updraft and matched with existing supercell conceptual models. With the ability to observe these key elements, forecasters successfully issued several tornado warnings prior to tornado development.

More recently, high-resolution (spatial and temporal) radar data collected by mobile radars have provided additional storm-scale information that can be used to refine and add to existing conceptual models. To date, all mobile radar data sets of tornadogenesis did not show intensification of the midlevel mesocyclone first followed by low-level mesocyclone intensification (i.e., TVS descent; French et al. 2013; French et al. 2014). Instead, the TVS built upwards or intensified at multiple heights simultaneously, suggesting that the conceptual model including TVS descent may be a result of temporal limitations of the current radar network (French et al. 2013). Other observations using mobile radars also emphasized the importance of low-level convergence along the secondary rear-flank gust front (e.g., Adlerman 2003; Wurman et al. 2007b; Kosiba et al. 2013) and during cyclic mesocyclogenesis (Dowell and Bluestein 2002). Though S-band radars may not always resolve the size of the features and processes observed by mobile radars, the knowledge acquired continues to refine conceptual models, which can be applied by forecasters during warning operations.

The National Weather Radar Testbed Phased-Array Radar (NWRT PAR, hereafter PAR) has also collected high-temporal resolution data at S-band that can help update existing conceptual models and be applied in an operational setting. Heinselman et al. (2008) demonstrated the ability of high-temporal resolution PAR data to better observe trends in features such as intensifying supercells and downbursts. Better observations of storm-scale trends could lead to refinements in existing conceptual models. In terms of operations, LaDue et al. (2010) conducted interviews with National Weather Service (NWS) forecasters and on-camera meteorologists to ascertain their wants and needs in terms of radar data. Many mentioned the need for faster update times and improved spatial resolution in order to adequately observe several storm-scale processes. In some instances, the forecasters knew how a storm was likely evolving by applying conceptual models, but the Weather Surveillance Radar-1988 Doppler (WSR-88D) network could not capture these trends. Heinselman et al. (2012) further confirmed this challenge by interviewing forecasters to determine the impact of rapid-scan radar data on their decision making process. Forecasters mentioned quick update times depicted more fluid-like storm evolutions that more closely matched with their conceptual model. This ability to better observe conceptual models increased forecaster confidence during the warning decision making process.

Previous PAR studies (e.g., Heinselman et al. 2012) have focused on the role of high-temporal resolution radar data in warning operations during marginal tornado events, though several questions remain unanswered especially in terms of how rapid-update radar data affects forecasters during outbreak scenarios. Therefore, the purpose of this study is to determine if high-temporal resolution PAR data may be advantageous to observing and applying tornadogenesis conceptual models from the viewpoint of a warning forecaster on 31 May 2013. On days with anticipated high-end severe weather, such as 31 May 2013, uncertainty exists as to whether or not rapid-scan radar data benefits a forecaster's tornado warning decision process. In these situations, the environmental conditions suggest enhanced tornado potential that can increase confidence in issuing tornado warnings earlier in a storm's lifecycle, potentially decreasing the impact of radar data on warning lead time (e.g., Moller et al. 1994; Andra et al. 2002). This particular case provides a unique opportunity to examine the potential benefits of rapid-update data in observing key features of a forecaster's conceptual model of tornadogenesis, by analyzing PAR data from about 40 min prior to tornadogenesis through the dissipation stage of the El Reno tornado (2221–2347 UTC). While high-temporal resolution radar data may not significantly impact *when* a forecaster ultimately warns during outbreak events, it could impact *how* a forecaster understands storm evolution in the context of his or her conceptual model. Better sampling of crucial conceptual model components may allow forecasters to more readily recognize potential threats and intelligently anticipate storm evolution (Andra et al. 2002) making them more able to effectively communicate threat to the general public. Additionally, the faster sampling time of the PAR could lead to more informed and more confident forecaster decisions (Heinselman et al. 2012; Heinselman et al. 2013) during the tornado warning process. These more informed decisions would ultimately add value to all components of a tornado warning including the polygon size and shape, updates to the warning (severe weather statements), cancellation of the warning, and the issuance and cancellation of tornado emergencies (OFCM 2010; NOAA 2012), which may be more likely during tornado outbreaks.

To focus the research on operational implications and forecaster perceptions, a warning forecaster who issued the El Reno tornado warnings was included in the research process. Input from the forecaster aided in the development of a detailed account of differences seen in the storm evolution depicted by PAR compared to the WSR-88D and the potential importance of these differences to his warning decision process had these data been available in operations.

## 2 Radar Data

KTLX is a mechanically steered S-band dual-polarization Doppler weather radar located near Oklahoma City, Oklahoma, USA, that is part of the Next Generation Radar Network used by the National Weather Service (Whiton et al. 1988). During this event, KTLX utilized volume coverage pattern (VCP) 212 (Brown et al. 2005), which provided an update time of about 4.5 min. The PAR is an electronically steered S-band Doppler research weather radar with vertical polarization (Zrnić et al. 2007). During this event, PAR utilized a modified VCP 12 which included an additional five elevation angles above 19.50° and provided an update time of 71 s.

## 3 Environmental Setting and Expectations

The 1800 UTC 31 May 2013 Norman sounding depicted an environment favorable for supercells with strong midlevel mesocyclones, very large hail and damaging winds (Fig. 1a). The sounding depicted an extremely unstable environment

(e.g., Doswell and Rasmussen 1994; Rasmussen and Blanchard 1998) with surface-based convective available potential energy exceeding 5000 J $kg^{-1}$ and low- and midlevel lapse rates of approximately 7–8 ºC $km^{-1}$, supporting optimal hail growth potential and intense updrafts. Deep-layer shear was also conducive to rapid storm organization and supercell development, with 0–6 km bulk shear in excess of 40–50 kt. Although the environment was weakly capped with only 74 J $kg^{-1}$ of convective inhibition in the mixed layer, several hours passed before storms formed around 2130 UTC. The one limiting factor for a greater tornado threat was weak storm relative helicity, owing to poor low-level shear at 1800 UTC, which limited the potential for vigorous low-level mesocyclones. Six hours later, the 0000 UTC Norman sounding revealed a more volatile environment (Fig. 1b). While strong instability and deep-layer wind shear were still present, comparison of the 1800 and 0000 UTC soundings revealed a substantial increase in 0–1-km and 0–3-km storm-relative helicity (from 113 $m^2 s^{-2}$ and 182 $m^2 s^{-2}$ at 1800 UTC to 294 $m^2 s^{-2}$ and 403 $m^2 s^{-2}$ at 0000 UTC, respectively) (Fig. 1b). The 0000 UTC sounding contained a more sickle-shaped wind profile supporting potential for strong to violent long-track tornadoes (e.g., Markowski et al. 2003; Esterheld and Guiliano 2008). Hodographs with this characteristic shape reveal environments containing greater low-level wind shear and an enhancement of low-level storm-relative inflow conducive to low-level mesocyclones and tornadogenesis (e.g., Brooks et al. 1993, 1994; Davies and Johns 1993; Kerr and Darkow 1996). This increase in low-level storm-relative helicity occurred as isallobaric flow backed in response to an area of low pressure at the intersection of a dryline and stalled front. Forecasters at the Storm Prediction Center and WFO Norman recognized this backing of surface winds as an indication that strong to violent tornado potential had significantly increased prior to storm initiation. Given the volatility of the environment and increasing confidence that significant severe weather would affect Oklahoma, staff at the WFO in Norman, Oklahoma determined that it was not a matter of if a violent tornado would occur, but a matter of when and where. This determination played a critical role throughout the warning decision process.

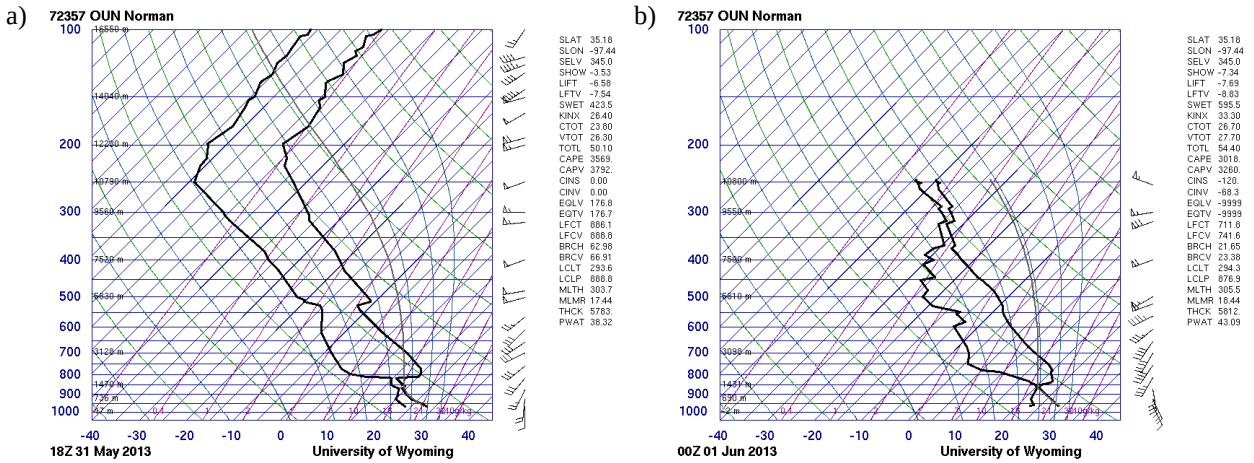


*Figure 1. a) 1800 UTC 31 May 2013 and b) 0000 UTC 1 June 2013 soundings launched in Norman, Oklahoma.*

## 4. Differences in PAR-Depicted Storm Evolution Significant to Operations

### 4.1 Initial Supercell Organization

In an environment strongly supportive of rapid storm organization and supercell development, an important consideration in the warning process is how quickly storms will organize, and, if multiple storms are present, which of them is most likely to produce significant severe weather. On 31 May 2013, the initial storms were rather numerous, so determining which one or ones deserved the most attention was difficult, especially when considering the latency of radar updates from KTLX.

A line of thunderstorms erupted around 2130 UTC along a stalled front draped from southwest to northeast across central Oklahoma. These storms became severe quickly, and the first severe thunderstorm warning was issued at 2146 UTC. Through time, many of the storms began to merge, with several disorganized storm clusters by 2214 UTC. As the storms continued to mature, attention turned to which storms would be most capable of producing tornadoes. This required a thorough investigation of low- and midlevel storm velocities and morphologies conducive to tornadogenesis. The most obvious culprit for potential tornado formation was the “tail-end Charlie” storm (A Comprehensive Glossary of Weather Terms for Storm Spotters – NWS SR-145) over Canadian County, west of Calumet, Oklahoma, which would go on to become the most significant storm of the day – the El Reno supercell. Signs of weak low-level rotation appeared with this conglomerate of convection as early as 2224 UTC but became more apparent by 2233 UTC, as low-level convergence tightened beneath a compact midlevel mesocyclone. Considering this swift intensification of the low-level circulation within a near storm environment highly supportive of rapid tornado development, confidence in imminent tornadogenesis was high and the first tornado warning was issued at 2236 UTC (Fig. 2). At 2305 UTC, 29 min after this initial tornado warning, the El Reno tornado began.

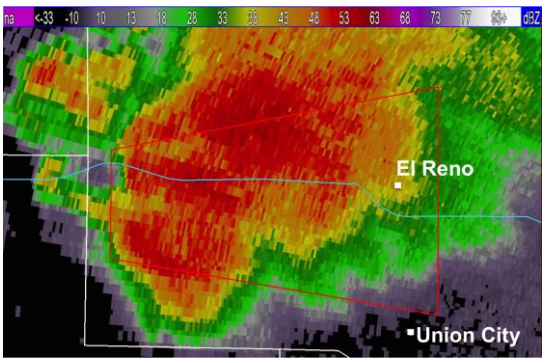


*Figure 2: KTLX (WSR-88D) 0.5° reflectivity field at 2237:46 UTC 31 May 2013 showing thunderstorm structure at issuance time of the initial tornado warning (solid red line).*

The El Reno supercell developed and intensified rapidly, so the increased temporal resolution provided by the PAR was crucial during the strengthening stages of the supercell from 2242 UTC to 2256 UTC. At 2242 UTC, a disorganized conglomerate of convection was apparent in reflectivity over western Canadian County, Oklahoma. Through 2252 UTC, PAR portrayed multiple small cell mergers occurring on the southern flank of this area of convection (Fig. 3a, c–f, h–k), indicating an intensification of low and midlevel inflow and increasing risk of tornadogenesis (e.g., Bunkers et al. 2005; Lee et al. 2006; Wurman et al. 2006). The KTLX radar provided only three volume scans during this length of time (Fig. 3b and l), making these features difficult to discern. With approximately one-minute updates, PAR provided a critical time advantage over KTLX in portraying these features during the storm's intensification. Velocity data from both PAR and KTLX showed some broad storm-scale rotation and a noted increase in both the magnitude and extent of the inflow region, with PAR again highlighting the uptick in inflow more readily (Fig 4). Between 2250 UTC and 2256 UTC, the development of a tight reflectivity gradient and high reflectivity band (e.g., Kulie and Lin 1998; Shabbot and Markowski 2005) became visible along the forward flank of the storm (Figs. 3 and 5). These features, along with a noted bounded weak echo region (BWER) in the upper levels, revealed a dramatic increase in the strength of the updraft. They also pointed to a likely increase in storm-scale rotation given the potential for tilting and stretching of ambient vorticity (e.g., Davies Jones et al. 2001). PAR again provided more timely data than KTLX during this period, enhancing awareness of the rapidly developing supercell and providing greater temporal detail to facilitate storm interrogation. This is significant because the development of the forward flank core and gradient in reflectivity, and subsequent strengthening of the updraft, corresponded to the first observed tornado with the El Reno storm at 2255 UTC.

### 4.2 Tornado Development

As the supercell continued to intensify, attention shifted to aspects of the storm conducive to tornado formation. For this purpose, the majority of radar interpretation occurred in the low levels (i.e. at or below 2.4°). Rotational magnitude of the low- and midlevel mesocyclones served as one of the primary indicators of potential tornadogenesis, as well as the perceived intensity of the updraft via the presence of certain radar signatures. During the early phases of supercell organization (2238–2256), rotation was not particularly strong, and the low level mesocyclone appeared rather broad, suggesting tornado potential was low. As the storm organized, vertical continuity of the mesocyclone increased confidence in possible tornadogenesis on multiple occasions (2233, 2247, and 2301). Evolution of the midlevel mesocyclone was also monitored for increasing tornado potential, with a notable intensification between 2247 and 2252. In addition, trends in the gate-to-gate velocity and RFD at the lowest elevation angle served as a proxy for mesocyclone intensity and possible tornadogenesis. Whereas early interrogation of the storm suggested low chances of tornado development, by 2306, strong low-level and midlevel rotation, in addition to other features such as an intense RFD, led to high confidence in the existence of a tornado, and concern that strong to violent tornado chances were on the rise.

Changes in the shape, spatial extent, and intensity of the supercell's inflow region were also important in the conceptual model of supercell strength and potential for tornado development. As the magnitude of the low-level inflow increased, confidence in the existence of a strong mesocyclone and associated updraft also increased. At 2242, the presence of strong inflow arcing into the vicinity of the mesocyclone indicated that a tornado would almost certainly develop, especially given the volatile near-storm environment. At 2301, a strong and fairly concentrated RFD converging with the intense inflow provided further confidence in imminent tornadogenesis. The intense inflow region observed at 2305 in KTLX data was indicative of a very strong updraft and greater potential in strong long-lived tornado potential. The rapid-update data provided by the PAR made it easier to observe and interpret the evolution of key features related to tornadogenesis. Specifically, the PAR's depiction of RFD surges and their interactions with the inflow region was less choppy than KTLX, making it easier to observe changes in these storm-scale features linked to tornado development.

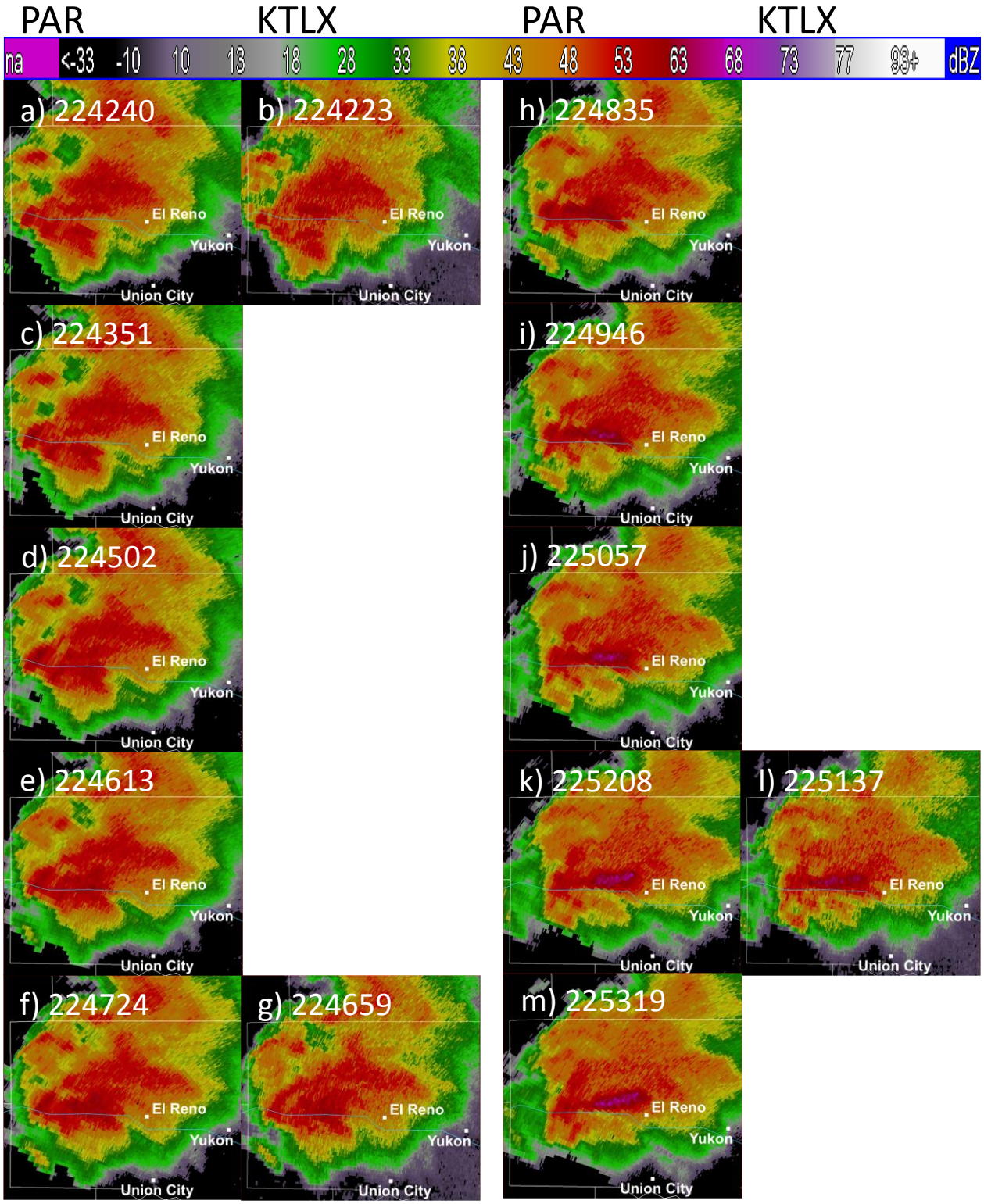


*Figure 3: 0.5° reflectivity field for PAR (left columns) and KTLX (right columns) on 31 May 2013 showing stages of supercell organization at a) 224240, b) 224223, c) 224351, d) 224502, e) 224613, f) 224724, g) 224659, h) 224835, i) 224946, j) 225057, k) 225208, l) 225137, and m) 225319. All times are in UTC. Reflectivity color bar for each image is located at the top of the figure.*

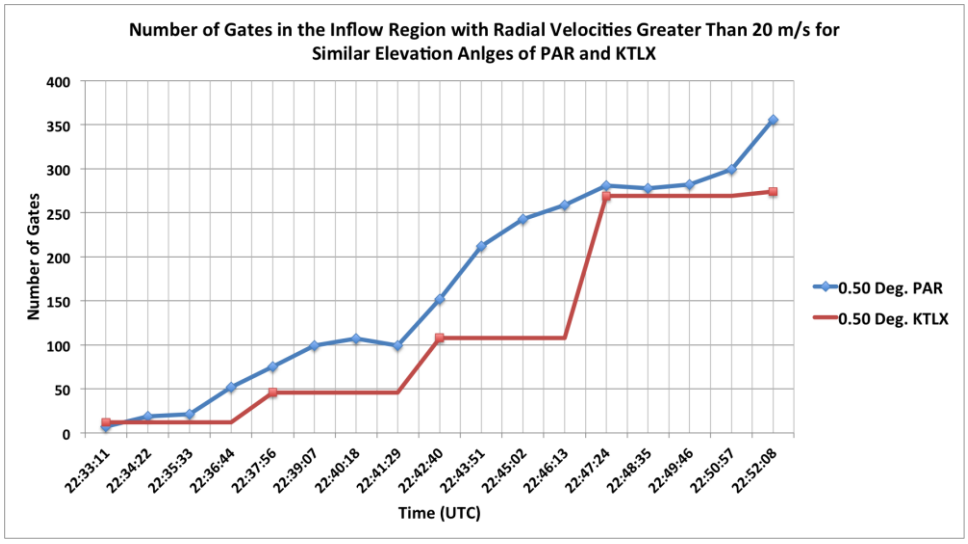


*Figure 4: Evolution of the spatial extent of winds greater than 20 m s-[1] (measured by number of gates) within the inflow region of the 31 May 2013 El Reno supercell sampled by PAR (blue line) and KTLX (red line) at 0.5° between 223311 and 225208 UTC.*

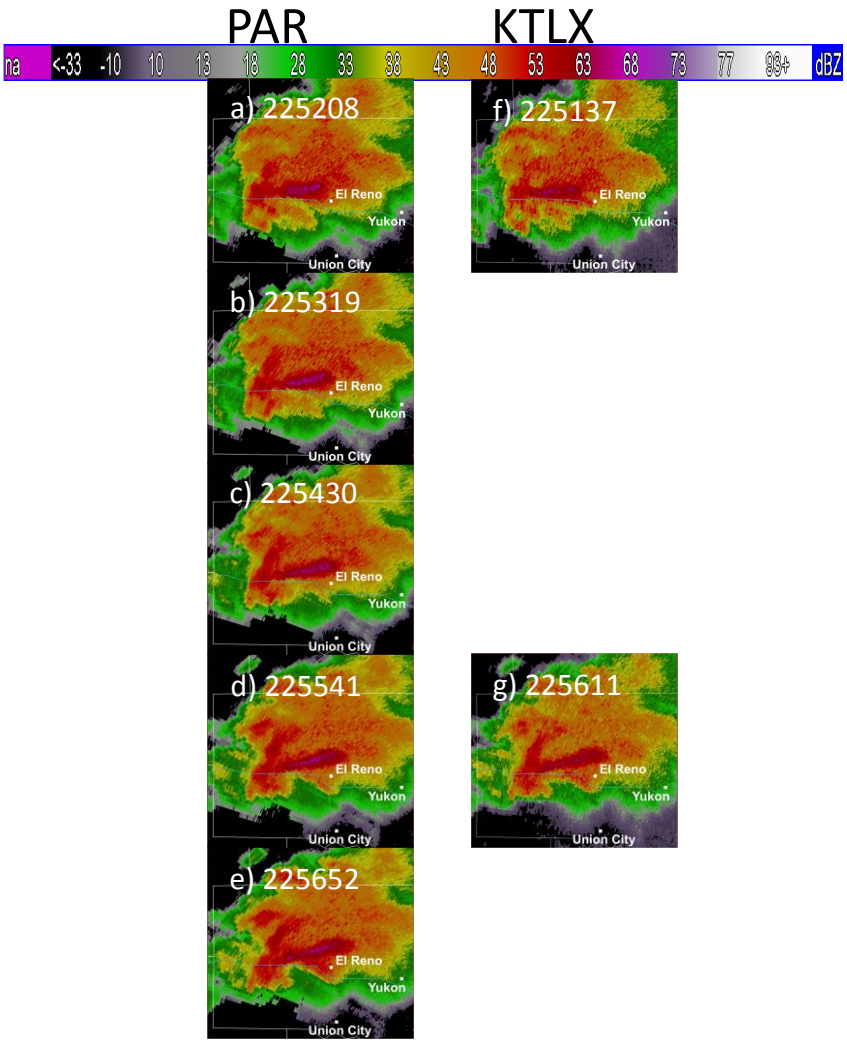


*Figure 5: 0.5° reflectivity field for PAR (left column) and KTLX (right column) on 31 May 2013 showing stages of supercell organization depicted by PAR at a) 225430, b) 225541, c), 225652, and KTLX at d) 225611. All times are in All times are in UTC. Reflectivity color bar for each image is located at the top of the figure.*

4.3 Rapid Changes in Motion of the Circulation and Tornado

Once a persistent low-level mesocyclone has formed, an accurate fix on the circulation and its expected motion are critical in developing warning polygons and providing timely location information. The tornado that struck areas between El Reno and Union City, Oklahoma displayed erratic changes in motion and forward speed throughout its life. These changes were not sampled well by KTLX, which often missed short-term variations in the motion of the tornadic circulation. From 2319 to 2324, the tornado made an abrupt northward turn, and PAR imagery clearly showed this progression (Fig. 6).

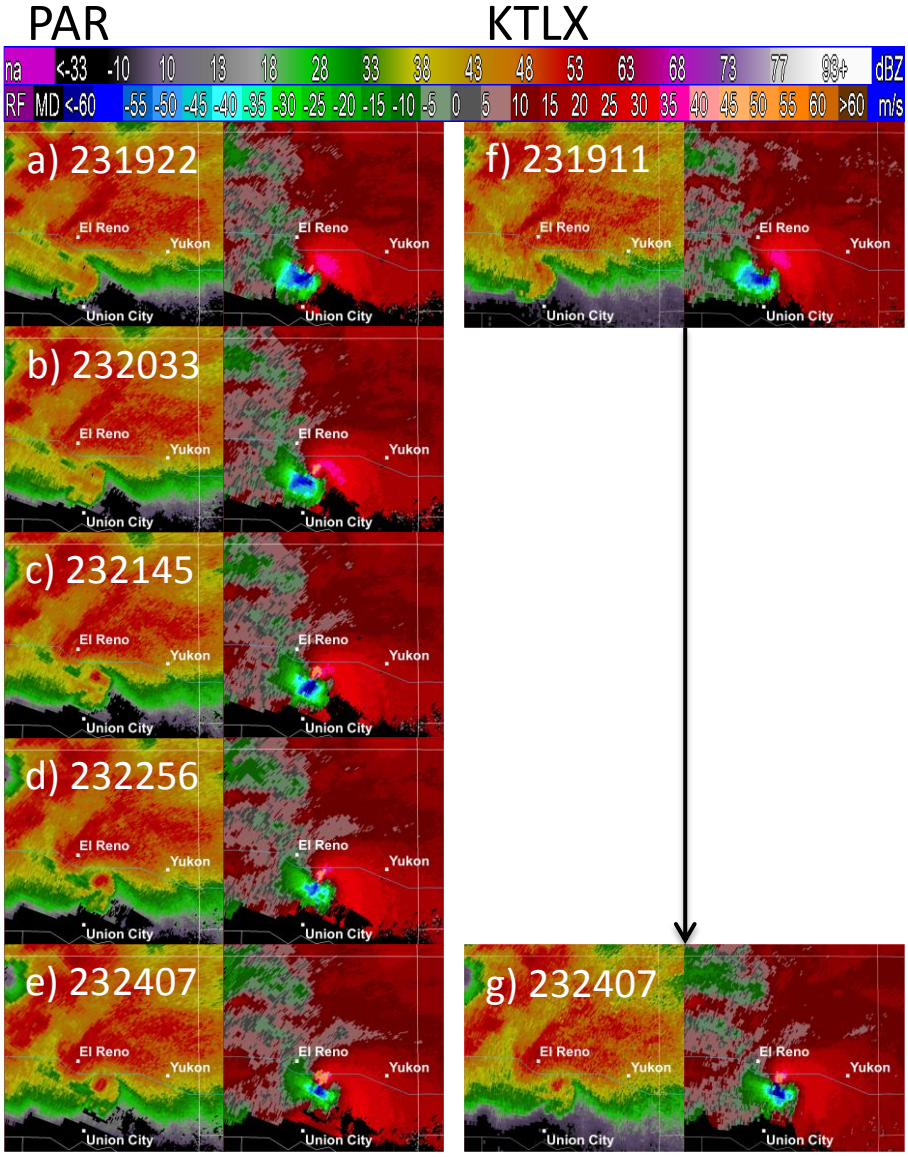


*Figure 6. 0.5° reflectivity and base velocity fields on 31 May 2013 showing tornado circulation motion as depicted by PAR at a) 231922, b) 232033, c) 232145, d) 232256, e) 232407, and KTLX at f) 231911 and g) 232407. All times are in UTC. Reflectivity and base velocity color bars are located at the top of the figure.*

KTLX, on the other hand, captured the circulation just before the tornado began its northward turn, with the subsequent scan coming in as the tornado ceased its northward motion. A similar evolution occurred from 2328 to 2333 as the tornadic circulation ceased its northward progress and stalled along Interstate 40 (Fig. 7). Both radars captured this deceleration, but PAR yielded more confidence, from the warning standpoint, in short-term tornado motion. KTLX volume scans were spaced such that the tornado appeared as though it might continue moving north after 2333, potentially venturing outside the existing warning polygon (Fig. 8). Consideration was given as to whether a new warning should be issued. Had PAR data been available, it would have been clear that the tornado had become nearly stationary, suggesting a new warning polygon was unnecessary. In addition, the one minute frequency in PAR scans would have allowed for more accurate estimated tornado locations and expected motion in updates to existing warnings. This became especially important once the first tornado emergency was issued for the Oklahoma City metropolitan area at 2328 as the storm and existing tornado continued moving toward more densely populated areas on the western outskirts of Oklahoma City.

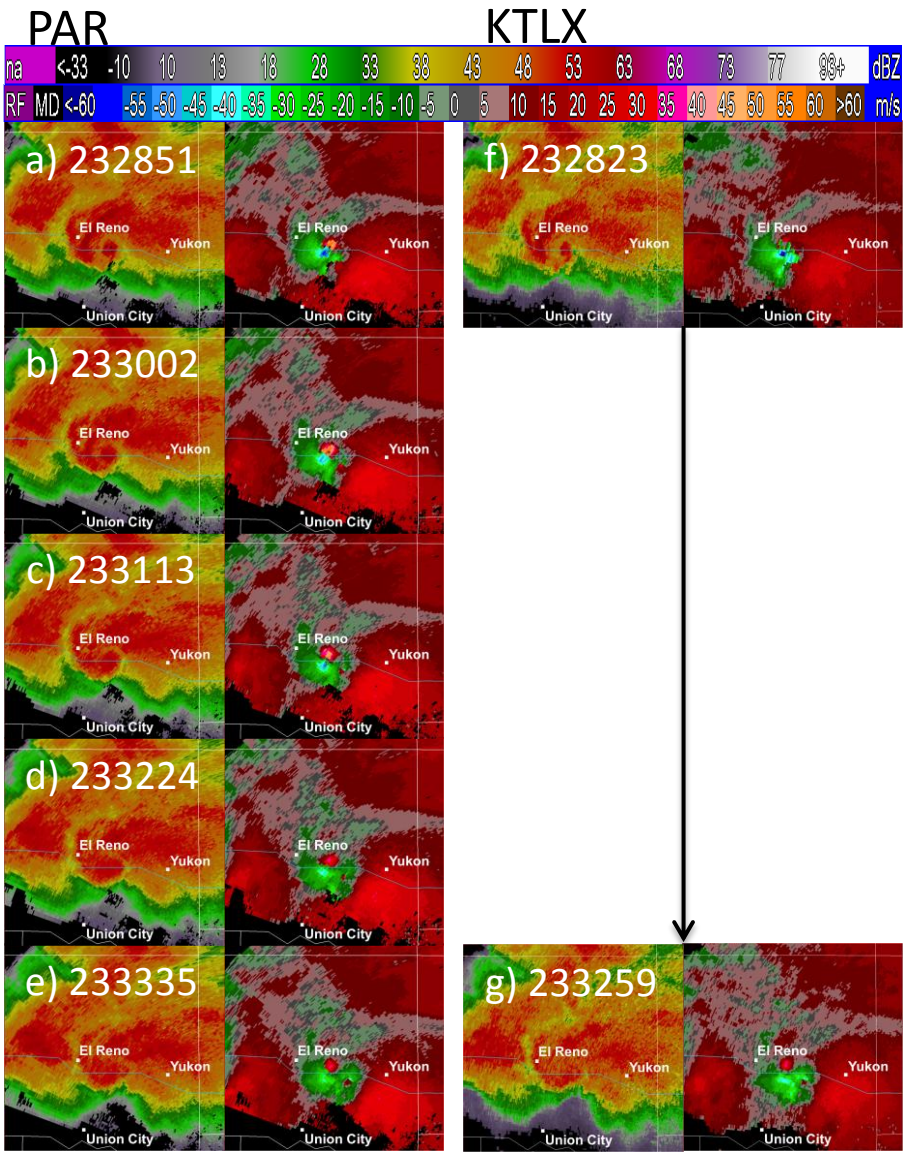


*Figure 7: 0.5° reflectivity and base velocity fields on 31 May 2013 showing nearly stationary tornado circulation motion as depicted by PAR at a) 232851, b) 233002, c) 233113, d) 233224, e) 233335, and KTLX at f) 232823 and g) 233259. All times are in UTC. Reflectivity and base velocity color bars are located at the top of the figure.*

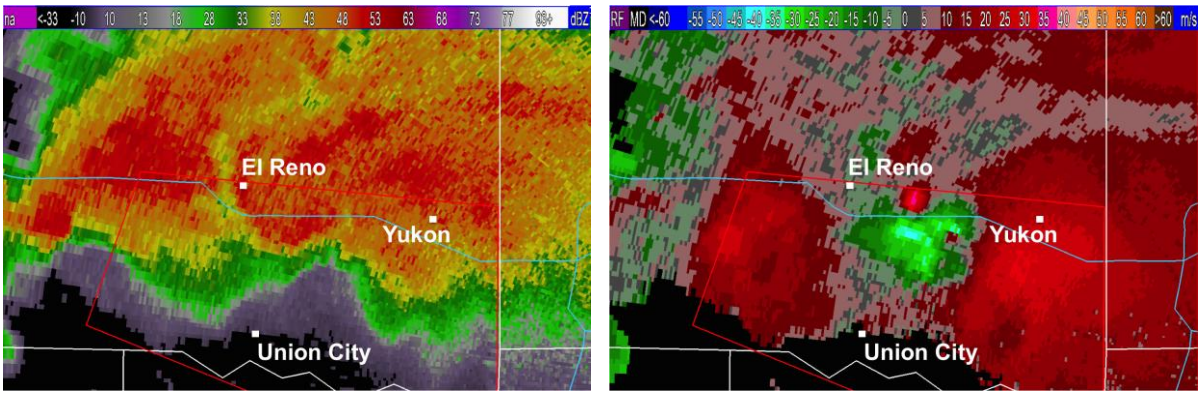


*Figure 8: KTLX 0.5° reflectivity field (left) and base velocity field (right) at 233259 UTC showing location of tornado circulation relative to tornado warning polygon (solid red line).*

When issuing tornado warnings, knowing when a tornado has shifted direction or speed is equally important as knowing when the tornado has stopped moving altogether. The short update-time for PAR would have provided a major advantage over KTLX in this realm as trends in motion and speed would have been more easily observed.

### 4.4 Merging Storms Cut Off Supercell Inflow

During high impact severe weather, it is important to frequently assess the environment and characteristics of ongoing convection to determine whether conditions remain supportive of severe weather. This can have a major bearing on operations and effective warning strategies through the duration of the event. This was a particularly important consideration on 31 May as the El Reno supercell and tornado were nearing western outskirts of the Oklahoma City Metropolitan Area.

Reflectivity trends during the early stages of the El Reno supercell suggested it might remain a dominant isolated supercell as it moved into Oklahoma City. As early as 2314 UTC, however, it became apparent that additional supercells were developing in close proximity to the El Reno storm. Understanding how storm interactions may impact the severity of a storm is crucial to the warning decision process. Some interactions favor an increase in tornado potential, such as storm mergers (e.g., Bunkers et al. 2005; Lee et al. 2006; Wurman et al. 2006), while others signify at least a temporary decline in the likelihood of tornadoes (e.g., Markowski et al. 2002).

At 2342, PAR and KTLX displayed a complex scenario with training supercells from near Yukon to west of El Reno. Assessing velocity data, both KTLX and PAR continued to show the persistent supercell characteristics of the El Reno storm, with broad inflow and a pronounced RFD. At this time, the El Reno tornado had fully occluded and was ongoing along Interstate 40 west of Yukon. With a single KTLX radar scan, it was unclear whether a second tornado would develop to the southeast of the occluded circulation within Oklahoma City limits, though it was apparent that another strong mesocyclone was developing. From 2343 to 2347, PAR revealed an RFD surge arching to the south and east over southeastern Canadian County (Fig. 9). KTLX data showed this feature, but with less clarity given the large lag in radar update times (Fig. 9). PAR data would have proven useful in the warning decision process as this RFD surge signified a period of reduced strong to violent tornado potential as the circulation became undercut, but an increased threat of widespread significant damaging winds. While a non-zero tornado threat certainly existed with the El Reno supercell as it marched into Oklahoma City, the knowledge of such an RFD surge may have been used in considering whether a second tornado emergency was necessary for the greater Oklahoma City Metropolitan Area.

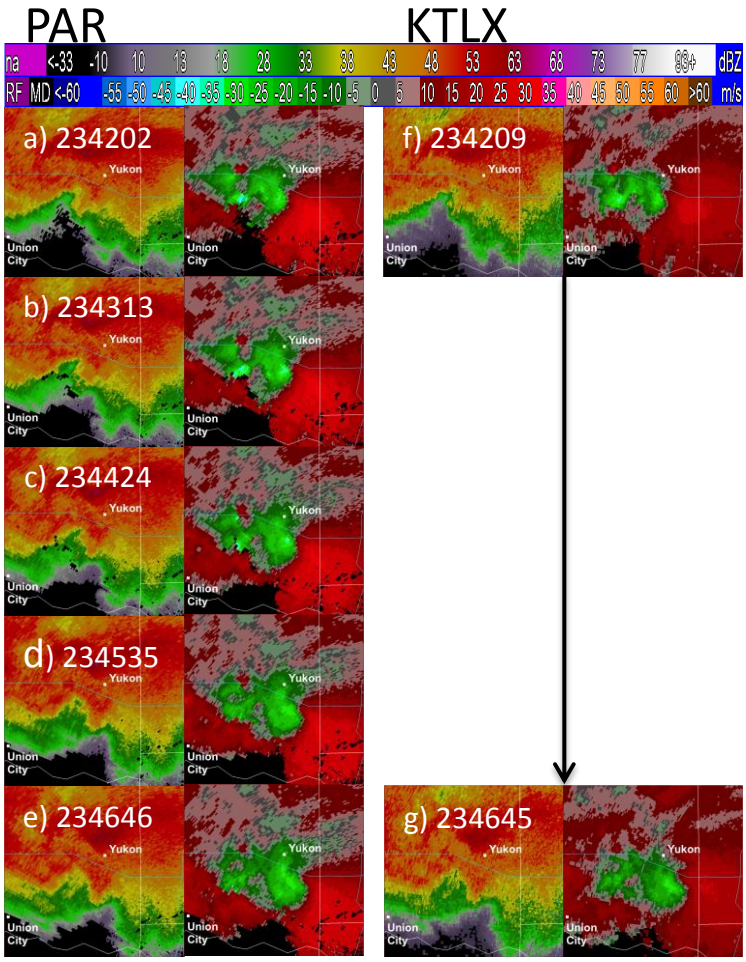


*Figure 30.5° reflectivity and base velocity fields on 31 May 2013 showing RFD surge as depicted by PAR at a) 234202, b) 234313, c) 234424, d) 234535, e) 234646, and KTLX at f) 234209 and g) 234645. All times are in UTC. Reflectivity and base velocity color bars are located at the top of the figure.*

In a setting where storm interactions play a key role in short- or long-term severe storm and tornado potential, PAR provides a major advantage over traditional Doppler radars. The one-minute update frequency of the PAR allows for greater situational awareness and more accurate assessment of supercell processes and complex storm morphologies, ultimately leading to better, more confident warning decisions.

*Acknowledgements:* The authors would like to thank Jeff Brogden, Karen Cooper, and Robert Toomey for their expertise with WDSSII and SOLO, Patrick Skinner for helping with radar data editing, and Emma Kuster for assistance with Python.

**References**

Adlerman, E. J., K. K. Droegemeier, and R. Davies-Jones, 1999: A numerical simulation of cyclic mesocyclogenesis. *J. Atmos. Sci.*, **56**, 2045–2069.

——, 2003: Numerical simulations of cyclic storm behavior: Mesocyclogenesis and tornadogenesis. Ph.D. dissertation, University of Oklahoma, 217pp.

Andra, D., L., E. M. Quoetone, and W. F. Bunting, 2002: Warning decision making: The relative roles of conceptual models, technology, strategy, and forecaster expertise on 3 May 1999. *Wea. Forecasting*, **17**, 559–566.

Bluestein, H. B., and C. R. Parks, 1983: A synoptic and photographic climatology of low-precipitation severe thunderstorms in the Southern Plains. *Mon. Wea. Rev.*, **111**, 2034–2046.

Brandes, E. A., 1978: Mesocyclone evolution and tornadogenesis: Some observations. *Mon. Wea. Rev.*, **106**, 995–1011.

——, 1984: Vertical vorticity generation and mesocyclone sustenance in tornadic thunderstorms: The observational evidence. *Mon. Wea. Rev.*, **112**, 2253–2269.

Brooks, H. E., C. A. Doswell III, and R. Davies-Jones, 1993: Environmental helicity and the maintenance and evolution of low-level mesocyclones. *The Tornado: Its Structure, Dynamics, Prediction, and Hazards, Geophys. Monogr.*, No. 79, Amer. Geophys. Union, 97–104.

——, ——, and R. B. Wilhelmson, 1994: The role of midtropospheric winds in the evolution and maintenance of low-level mesocyclones. *Mon. Wea. Rev.*, **122**, 126–136.

——, and ——, 1994: On the environments of tornadic and nontornadic mesocyclones. *Wea. Forecasting*, **9**, 606–618.

Brown, R. A., L. R. Lemon, and D. W. Burgess, 1978: Tornado detection by pulsed Doppler radar. *Mon. Wea. Rev.* **106**, 29–38.

——, R. A., V. T. Wood, R. M. Steadham, R. R. Lee, B. A. Flickinger, and D. Sirmans, 2005: New WSR-88D volume coverage pattern 12: Results of field tests. *Wea. Forecasting*, **20**, 385–393.

——, R. M. Steadham, B. A. Flickinger, R. R. Lee, D. Sirmans, and V. T. Wood, 2005: New WSR-88D voume coverage pattern 12: Results of field tests. *Wea. Forecasting*, **20**, 385–393.

Bunkers, M. J., M. R. Hjelmfelt, and P. L. Smith, 2006: An observational examination of long-lived supercells. Part I: Characteristics, evolution, and demise. *Wea. Forecasting*, **21**, 673–688.

Burgess, D. W., K. E. Wilk, J. D. Bonewitz, K . M. Glover, D. W. Holmes, and J. Hinkelman, 1979: Doppler radar: The Joint Doppler Operational Project. *Weatherwise*, **32**, 72–75.

——, and L. R. Lemon, 1990: Severe thunderstorm detection by radar. *Radar in Meteorology*, D. Atlas, Ed., Amer. Meteor. Soc., 619–647.

——, ——, and R. A. Brown, 1975: Tornado characteristics revealed by Doppler Radar. *Geophys. Res. Lett.*, **2**, 183–184.

Davies, J. M., and R. H. Johns, 1993: Some wind and instability parameters associated with strong and violent tornadoes. 1. Wind shear and helicity. *The Tornado: Its Structure, Dynamics, Prediction, and Hazards, Geophys. Monogr.*, No. 79, Amer. Geophys. Union, 573–582.

Davies-Jones, R., R. J. Trapp, and H. B. Bluestein, 2001: Tornadoes and tornadic storms. *Severe Convective Storms, Meteor. Monogr.*, No. 50. Amer. Meteor. Soc., 167–221.

Doswell, C. A., III, and D. W. Burgess, 1993: Tornadoes and tornadic storms: A review of conceptual models. *The Tornado: Its Structure, Dynamics, Prediction,and Hazards, Geophys. Monogr.*, No. 79, Amer. Geophys. Union, 161–172.

——, and E. N. Rasmussen, 1994: The effect of neglecting the virtual temperature correction on CAPE calculations. *Wea. Forecasting*, **9**, 625–629.

——, H. E. Brooks, and R. A. Maddox, 1996: Flash flood forecasting: An ingredients-based methodology. *Wea. Forecasting*, **11**, 560–581.

Dowell, D. C., and H. B. Bluestein, 2002: The 8 June 1995 McLean, Texas storm. Part I: Observations of cyclic tornadogenesis. *Mon. Wea. Rev.*, **130**, 2626–2648.

Dunn, L. B., 1990: Two examples of operational tornado warnings using Doppler radar data. *Bull. Amer. Meteor. Soc.*, **71**, 145–153.

Esterheld, J. M., and D. J. Guiliano, 2008: Discriminating between tornadic and non-tornadic supercells: A new hodograph technique. *Electronic J. Severe Storms Meteor.*, **3** (2), 1–50.

French, M. M., H. B. Bluestein, I. PopStefanija, C. A. Baldi, R. T. Bluth, 2013: Reexamining the vertical development of tornadic vortex signatures in Supercells. *Mon. Wea. Rev.*, **141**, 4576–4601.

——, ——, ——, ——, and ——, 2014: Mobile, phased-array, Doppler radar observations of tornadoes at X band. *Mon. Wea. Rev.*, **142**, 1010–1036.

Hahn, B. B., E. Rall, and D. W. Klinger, 2003: Cognitive task analysis of the warning forecaster task. Rep. RA1330-02-SE-0280. [Available from Klein Associated Inc., 1750 Commerce Center Blvd., North Fairborn, Ohio 45324-6362.]

Heinselman, P. L., D. L. Priegnitz, K. L. Manross, T. M. Smith, and R. W. Adams, 2008: Rapid sampling of severe storms by the National Weather Radar Testbed Phased Array Radar. *Wea. Forecasting*, **23**, 808–824.

——, D. S. LaDue, and H. Lazrus, 2012: Exploring impacts of rapid-scan radar data on NWS warning decisions. *Wea. Forecasting*, **27**, 1031–1044.

——, ——, D. M. Kingfield, R. Hoffman, and B. W. MacAloney II, 2013: Simulated NWS tornado warning decisions using rapid-scan radar data. Preprints, *29th Conf. Environ. Info. Processing Technologies*, Austin, TX, Amer. Meteor. Soc., 8.3. [Available at https://ams.confex.com/ams/93Annual/webprogram/Paper219547.html.]

Johns, R. H., and C. A. Doswell, 1992: Severe Local Storms Forecasting. *Wea. Forecasting*, **7**, 588–612.

Johns, R. H., 1993: Meteorological conditions associated with bow echo development in convective storms. *Wea. Forecasting*, **8**, 294–299.

Kerr, B. W., and G. L. Darkow, 1996: Storm-relative winds and helicity in the tornadic thunderstorm environment. *Wea. Forecasting*, **11**, 489–505.

Klemp, J. B., and R. Rotunno, 1983: A study of the tornadic region within a supercell thunderstorm. *J. Atmos. Sci.*, **40**, 359–377.

Kosiba, K., J. Wurman, Y. Richardson, P. Markowski, P. Robinson, and J. Marquis, 2013: Genesis of the Goshen County, Wyoming tornado on 5 June 2009 during VORTEX2. *Mon. Wea. Rev.*, **141**, 1157–1181.

Kulie, M. S., and Y.-L. Lin, 1998: The structure and evolution of a numerically simulated high-precipitation supercell thunderstorm. *Mon. Wea. Rev.*, **126**, 2090–2116.

LaDue, D. S., P. L. Heinselman, and J. F. Newman, 2010: Strengths and limitations of current radar systems for two stakeholder groups in the Southern Plains. *Bull. Amer. Meteor. Soc.*, **91**, 899–910.

Lee, B. D., B. F. Jewett, and R. B. Wilhelmson, 2006: The 19 April 1996 Illinois tornado outbreak. Part II: Cell mergers and associated tornado incidence. *Wea. Forecasting*, **21**, 449–464.

——, C. A. Finley, and T. M. Samaras, 2008: Thermodynamic and kinematic analysis near and within the Tipton, KS tornado on May 29 during TWISTEX 2008. Preprints, *24th Conf. on Severe Local Storms*, Savannah, GA, Amer. Meteor. Soc., P3.13. [Available online at http://ams.confex.com/ams/pdfpapers/142078.pdf.]

Lemon, L. R., D. W. Burgess, and R. A. Brown, 1978: Tornadic storm airflow and morphology derived from single-Doppler radar measurements. *Mon. Wea. Rev.*, **106**, 48–61.

Lindley, T., and G. Morgan, 2004: The Pecos County, Texas hail storms of 10 May 2002: A null tornado event from a warning decision perspective. *Electronic J. of Operational Meteor.*, **1**.

Markowski, P. M., J. M. Straka, and E. N. Rasmussen, 2002: Direct surface thermodynamic observations within the rear-flank downdrafts of nontornadic and tornadic supercells. *Mon. Wea. Rev.*, **130**, 1692–1721.

——, C. Hannon, J. Frame, E. Lancaster, and A. Pietrycha, 2003: Characteristics of vertical wind profiles near supercells obtained from the Rapid Update Cycle. *Wea. Forecasting*, **18**, 1262–1272.

Moller, A. R., C. A. Doswell III, and R. Przybylinski, 1990: High-precipitation supercells: A conceptual model and documentation. Preprints, *16th Conf. on Severe Local Storms*, Kananaskis Park, AB, Canada, Amer. Meteor. Soc., 52–57.

——, C. A. Doswell III, M. P. Foster, and G. R. Woodall, 1994: The operational recognition of supercell thunderstorm environments and storm structures. *Wea. Forecasting*, **9**, 327–347.

NOAA, 2012: WFO severe weather products specification. [Available at http://www.nws.noaa.gov/directives/010/010.htm]

NWS Performance Management, 2013: [Available at https://verification.nws.noaa.gov/]

OFCM, 2010: National severe local storms operations plan. [Available at http://www.ofcm.gov/slso/2010/slso2010.htm.]

Rasmussen, E. N., and D .O. Blanchard, 1998: A baseline climatology of sounding-derived supercell and tornado forecast parameters. *Wea. Forecasting*, **13**, 1148–1164.

Shabbott, C. J., and P. M. Markowski, 2006: Surface in situ observations within the outflow of forward-flank downdrafts of supercell thunderstorms. *Mon. Wea. Rev.*, **134**, 1422–1441.

Vasiloff, S. V., 2001: Improving tornado warnings with the Federal Aviation Administration's Terminal Doppler Weather Radar. *Bull. Amer. Meteor. Soc.*, **82**, 861–874.

Whiton, R. C., P. L. Smith, S. G. Bigler, K. E. Wilk, and A. C. Harbuck, 1998: History of operational use of weather radar by U.S. weather services. Part II: Development of operational Doppler weather radars. *Wea. Forecasting*, **13**, 244–252.

Wicker, L., J., and R. B. Wilhelmson, 1995: Simulation and analysis of tornado development and decay within a three-dimensional supercell thunderstorm. *J. Atmos. Sci.*, **52**, 2675–2703.

Wilson, J., R. Carbone, H. Baynton, and R. Serafin, 1980: Operational application of meteorological Doppler radar. *Bull. Amer. Meteor. Soc.*, **61**, 1154–1168.

Wurman, J., Y. Richardson, C. Alexander, S. Weygandt, and P. F. Zhang, 2007a: Dual- Doppler and single-Doppler analysis of a tornadic storm undergoing mergers and repeated tornadogenesis. *Mon. Wea. Rev.*, **135**, 736–758.

——, ——, ——, ——, and ——, 2007b: Dual-Doppler analysis of winds and vorticity budget terms near a tornado. *Mon. Wea. Rev.*, **135**, 2392–2405.

Zrnić, D. S., J. F. Kimpel, D. E. Forsyth, A. Shapiro, G. Crain, R. Ferek, J. Heimmer, W. Benner, T. J. McNellis, and R. J. Vogt, 2007: Agile beam phased array radar for weather observations. *Bull. Amer. Meteor. Soc.*, **88**, 1753–1766.